Pergamon

PII: S0148-9062(96)00053-8

Int. J. Rock Mech. Min. Sci. Vol. 34, No. 1, pp. 3–16, 1997

0148-9062/97 $17.00 + 0.00

Laboratory Investigation of the Mechanical Behaviour of Tournemire Shale

H. NIANDOU†
J. F. SHAO†‡
J. P. HENRY†
D. FOURMAINTRAUX§

This paper presents laboratory investigations of the mechanical behaviour of a typical anisotropic rock: Tournemire shale. Hydrostatic compressibility tests allowed characterization of the structural anisotropy of the material. Triaxial compression tests, including unloading cycles, were performed. Anisotropic elastic response, plastic deformation and failure behaviour have been investigated. The elastic behaviour of the shale is non-linear and the shale exhibits large anisotropic plastic deformation. The failure behaviour of the shale is anisotropic and strongly depends on confining pressure and loading orientation. © 1997 *Elsevier Science Ltd. All rights reserved.*

1. INTRODUCTION

Many underground works, such as chemical and nuclear waste storage and oil boreholes, are located in anisotropic rocks. The design and stability analysis of such structures require a knowledge of the deformation and failure of these rock materials. Much research has been conducted on anisotropic rocks, including experimental characterization, theoretical studies and numerical modelling. Different topics have been covered, such as micro- and macro-structural factors in anisotropy, interaction between inherent and induced anisotropies, failure mechanisms and strength parameters, influences of hydrostatic pressure, plastic deformation and damage, stress measurement in anisotropic media and characterization of elastic parameters. From experimental data, various kinds of models have been developed for the description of the deformation and failure of anisotropic rocks. Different approaches have been proposed, empirical models by introducing the variations of material parameters with the loading orientation in isotropic models, mathematical models by using the theory of representation of tensor functions.

It is not the purpose of this paper to establish an exhaustive summary of the works devoted to anisotropic rocks. We mention only some review papers addressing the state of art on the study of anisotropic materials [1–6]. Complete lists of references were given in these papers.

Among anisotropic rocks, the group of sedimentary rocks, termed shales, represents a particular interest in nuclear waste storage and oil industry. Experimental investigations are still necessary to have a better understanding of the mechanical behaviour of these materials. Indeed, according to recent surveys [7], in the oil industry, wellbore stability problems represent an extra drilling cost of up to 15% and 80% of such problems occur in shales (although this term covers a large variety of rocks). The shales are anisotropic in deformability and the failure mode is due to their sedimentary structure. This means that much more complex models should be used to describe their mechanical behaviour. Moreover, these rocks are of low porosities and permeabilities, and time dependent effects such as pressure diffusion and ionic convection have to be considered. Capillary effects between diphasic fluids could play an important role [7, 8].

The present work was included in the framework of a general research program devoted to wellbore instability in shales (STAR), jointly conducted by three French oil companies and institutions (ELF-Aquitaine, TOTAL and IFP). The main aim was to carry out extensive laboratory experiments on the mechanical

†Laboratoire de Mécanique de Lille, URA 1441 CNRS, Université de Lille I, Eudil, 59655 Villeneuve d'Ascq Cedex, France.
‡Author to whom correspondence should be addressed.
§ELF Aquitaine Production, Centre Scientifique et Technique Jean Féger, Avenue Larribau, 64018 Pau Cedex, France.

Table 1. Porosity and density vs temperature [8]

Temperature	Porosity	Density
65°	8.35%	2.72
80°	8.53%	2.73
150°	13.7%	2.76

behaviour of Tournemire shale. The emphasis is given to investigating elastic response, plastic flow and failure behaviour of the shale. Experimental results presented in this part provide a data base for the development of elastoplastic modelling and failure criteria.

2. DESCRIPTION OF TOURNEMIRE SHALE

The rock studied is an upper Toarcian massive shale taken from the Tournemire site in the Massif Central, France. The mineralogical composition is: 27.5% kaolinite, 16.5% illite, 19% quartz, 15% calcite, 2.7% chlorite, 8.3% I/S (interstratifier) and 11% others (pyrite, siderite, feldspars . . .). The porosity and density at different temperatures are given in Table 1.

The native water content in the shale varies from 4.5 to 8% [8]. In order to avoid the modification of the water content and keep the shale in the state as close as possible to that *in situ*, the shale blocks from the site were covered by a waterproof coating (Rubson) until preparation of samples in the laboratory. Samples were bored with air pressure and prepared with caution to avoid disturbing the material.

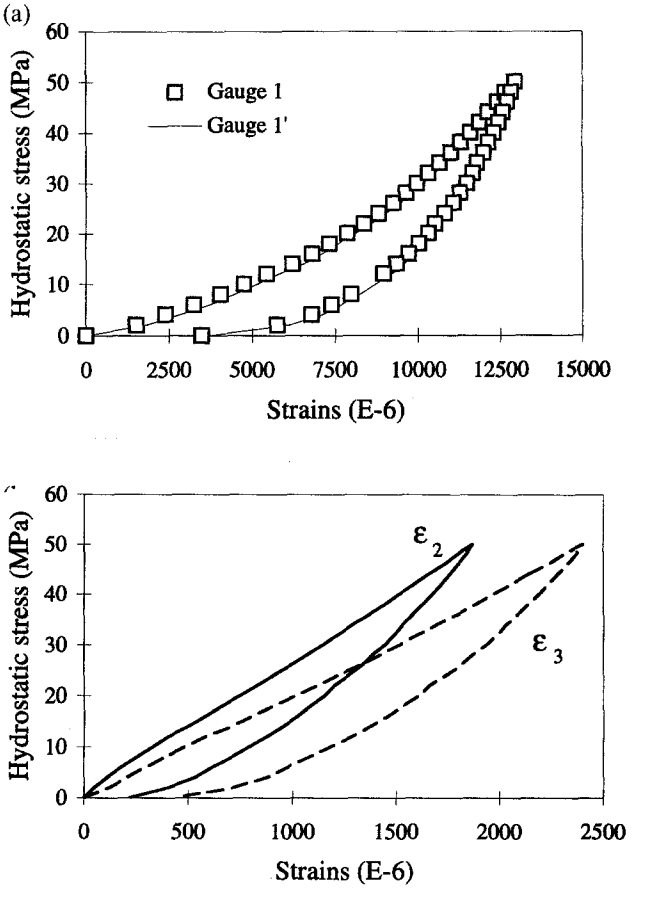

Fig. 2. (a) Strain in the direction S_1 normal to bedding plane during compressibility test. (b) Strains in the directions S_1 and S_2 parallel to bedding plane during compressibility test.

3. COMPRESSIBILITY TESTS

Hydrostatic compression tests were used to identify the anisotropic structure of Tournemire shale. A general way to characterize the kind of anisotropy is the dynamic test method. However, this method characterizes the elastic response of material rather than the global behaviour including plastic deformation and damage. In addition, it requires samples of a particular shape which are difficult to obtain for this shale. As bedding planes are relatively easy to identify in Tournemire shale, it is simpler to conduct hydrostatic compression tests on cubic samples cut according to apparent bedding planes. Let us define a coordinate system (S_1, S_2, S_3) attached to the stratified structure of the shale so that the S_1 axis is normal to bedding planes which are defined by two axes (S_2, S_3) (Fig. 1). The size of the cubic samples is 5 cm. Strains in the three directions of the structural reference were measured by six strain gauges (two per direction) as shown in Fig. 1. Samples were protected with silicon and placed in a cell. In this way, the tests were performed under undrained conditions and with the natural state of saturation. Several tests were carried out [9], we present the main results obtained from these tests here.

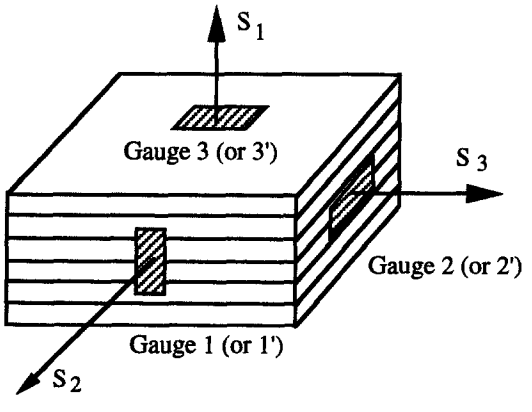

Fig. 1. Structural coordinate and strain gauge position in compressibility test.

In Fig. 2(a) and (b), strains in three directions are shown. In Fig. 2(a), we can see that the values of strain ε_1 measured by the two gauges on two opposite sides are nearly identical. This implies that the deformation of Tournemire shale is quite homogeneous. By comparing strains in three directions, it is seen that the strain in direction S_1 is much greater than those in the other two directions (S_2, S_3), and these last two are quite similar. This means that it is reasonable to assume that the shale behaviour is transversely isotropic. The main anisotropic direction is S_1 and the shale behaviour in the bedding planes is quite isotropic. Moreover, the large strain in direction S_1 is due to closure of bedding planes under compressive stress.

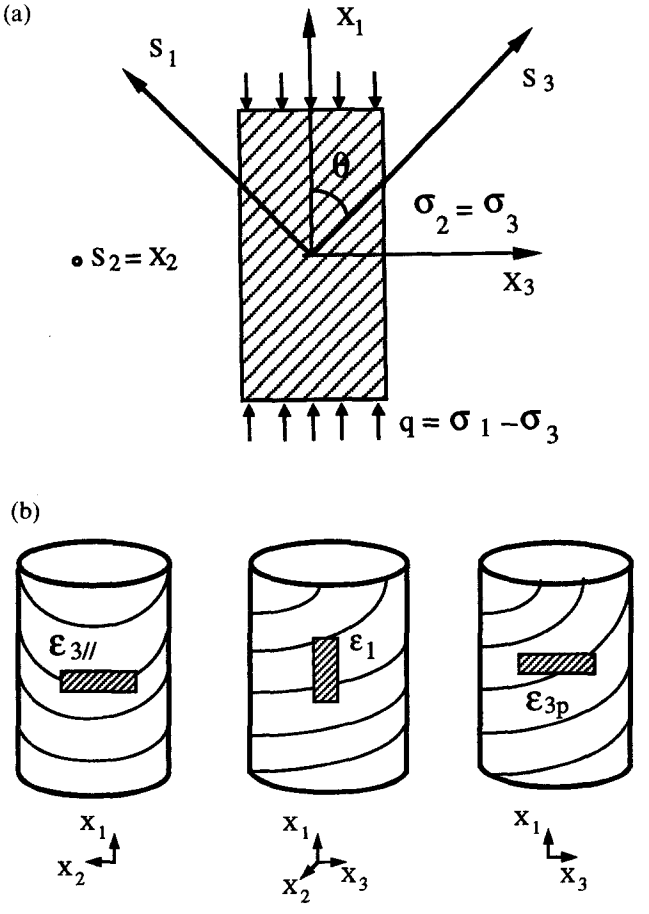

Fig. 3. (a) Definition of loading orientation θ. (b) Positions of strain gauges in triaxial compression test.

The strains in three directions are non-linear, especially ε_1. After removing the applied stress, important irreversible strains are obtained and these are also anisotropic in three directions. The principal plastic strain of the shale under hydrostatic compression is due to irreversible closure of bedding planes. In addition, unloading cycles were performed during some tests, it was noticed that the bulk modulus increases with hydrostatic stress [9]. However, for anisotropic media, the bulk modulus is not a representative material constant as it does not show the directional character of material.

4. TRIAXIAL TESTS

4.1. Presentation of tests

Conventional triaxial tests were performed on cylindrical samples of 37 mm in diameter and 75 mm in height (approximately). This sample size seems correct with regard to heterogeneity of this fine grained rock. Loading orientation is defined by the angle θ between the bedding planes and the axial stress σ_1 [Fig. 3(a)].

Strains of samples were measured by means of strain gauges and their positions are illustrated in Fig. 3(b). Two gauges are oriented in the X_1 direction corresponding to axial loading. These gauges allow one to measure the longitudinal strains of the sample. Their average value is termed ε_1. Two strain gauges are oriented in the X_2 $(=S_2)$ direction which is parallel to the bedding planes. These measure the transversal strains which are parallel to the bedding planes and their average value is noted $\varepsilon_{3//}$. Finally, two other gauges are oriented in the perpendicular direction of the bedding planes X_3, and measure the transversal strains which are perpendicular to the bedding planes. Their average value is noted ε_{3p}. For tests in $\theta = 90°$, only two longitudinal gauges and two transversal gauges were used, because in this case we have $\varepsilon_{3//} = \varepsilon_{3p}$.

Two series of tests were performed, monotonic tests and tests with unloading–reloading cycles. Various loading orientations and confining pressures were considered to obtain quite a complete data base for the studied shale. The list of orientations and confining pressures is given as follows:

$$\theta = 0°, 15°, 20°, 30°, 45°, 60°, 75°, 90°$$

$$\sigma_3 = 1, 5, 10, 20, 30, 40, 50 \text{ MPa}.$$

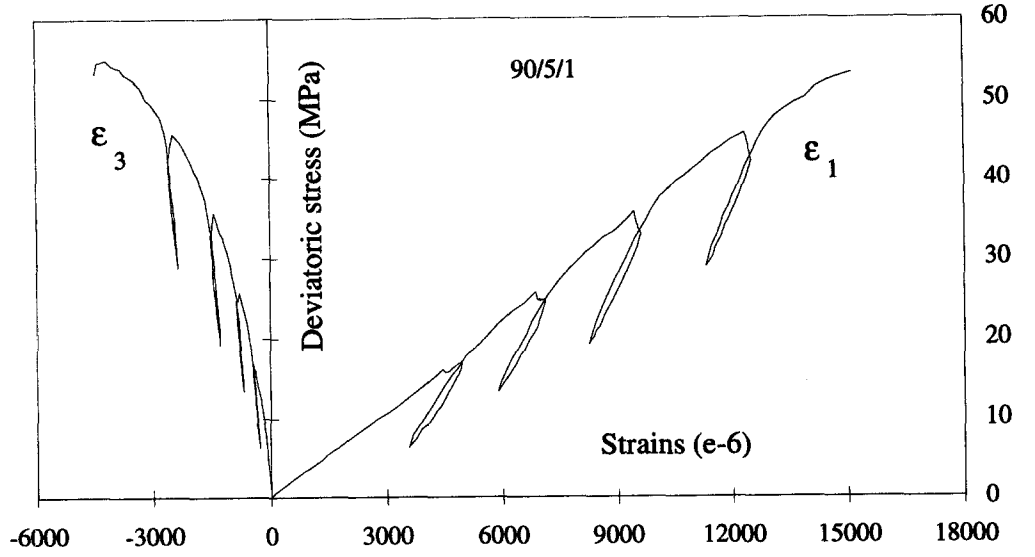

Fig. 4. Stress–strain curves during triaxial test with $\theta = 90°$ and 5 MPa confining pressure.

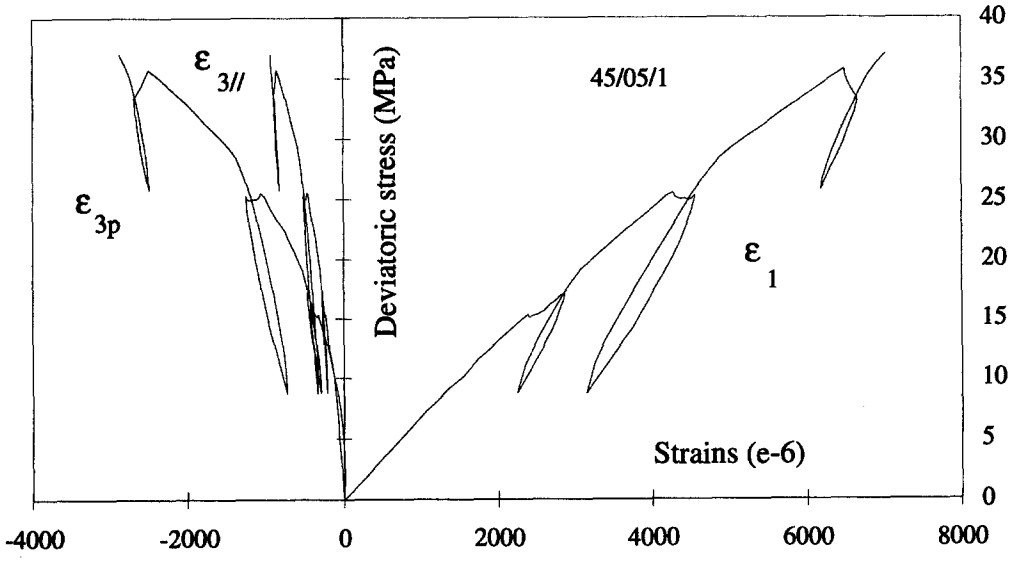

Fig. 5. Stress–strain curves during triaxial test with $\theta = 45°$ and 5 MPa confining pressure.

More than 50 tests were performed. In order to easily identify each test, a notation composed of three numbers was used: loading orientation θ, confining pressure σ_3 and series number n. In this paper, it is not necessary to analyze each test and the complete experimental results have been presented in ref. [9]. We will only present the significant results obtained from these tests.

4.2. Main results and general analyses

In each test, axial and lateral strains were measured as a function of deviatoric stress. In Figs 4–6, typical stress–strain curves are shown for three representative orientations and confining pressures. In this section, we will make some general remarks about the anisotropic properties of strains, the volumetric compressibility and dilatancy, as well as the hardening and softening behaviour of the shale. Detailed discussions for different topics will be covered in the following sections.

(1) For orientations other than 90°, the two lateral strains, respectively, parallel ($\varepsilon_{3//}$) and perpendicular (ε_{3p}) to the bedding planes, are very different. This confirms that the shale behaviour is anisotropic in nature. Moreover, the lateral strain (ε_{3p}) is systematically greater than the other one ($\varepsilon_{3//}$). This means that the deformability of the bedding planes (sliding and extension) plays an important role in the deformation of the shale.

(2) Stress–strain relationships are non-linear and irreversible. After the removal of deviatoric stress, the plastic deformation represents about 50% of the total deformation for both axial and lateral strains. The plastic strains are also anisotropic in nature.

(3) In Fig. 7(a–c), we show axial strains vs deviatoric stress for three orientations and various confining pressures. It is obvious that the behaviour of the shale is pressure sensitive. For nearly all the tests shown, there is a closure phase of initial fractures at the starting of

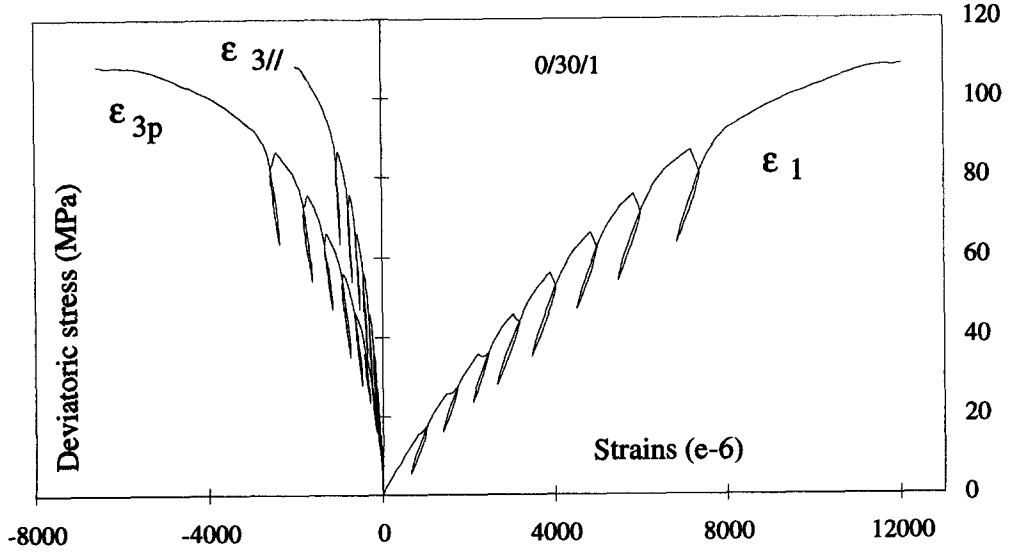

Fig. 6. Stress–strain curves during triaxial test with $\theta = 0°$ and 30 MPa confining pressure.

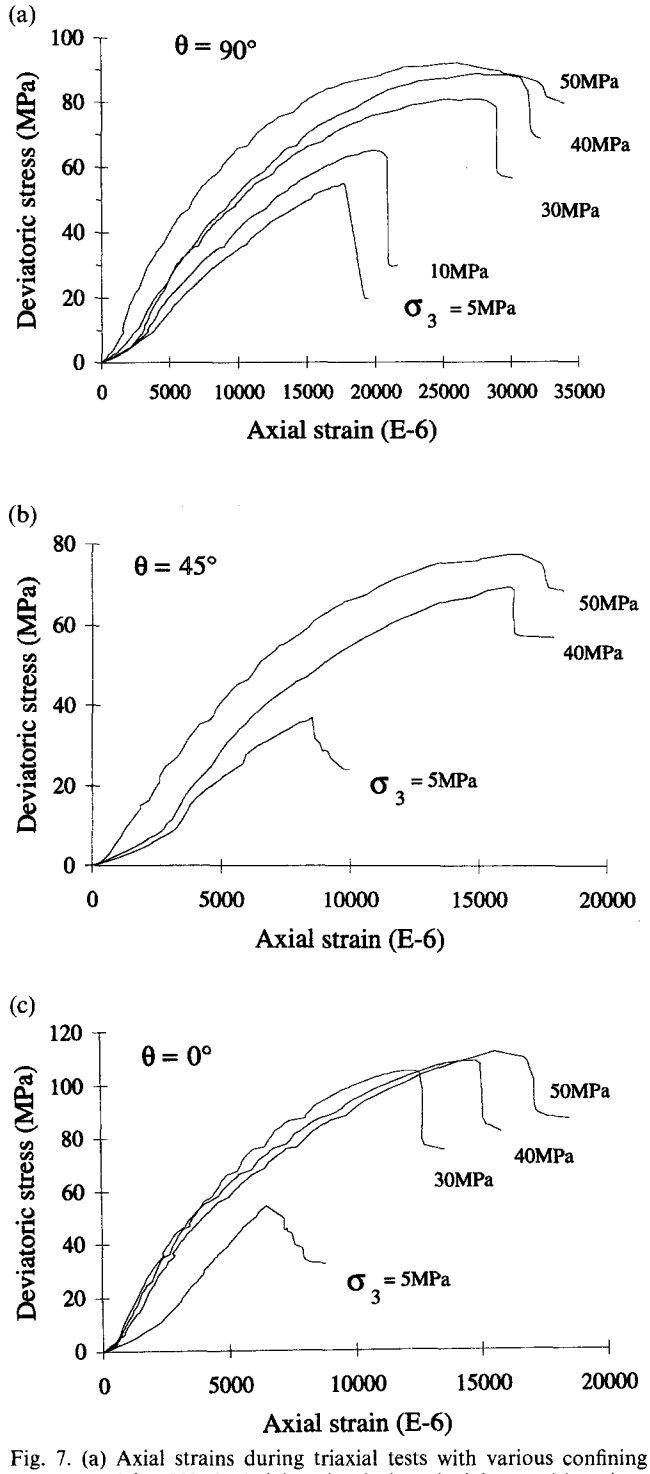

Fig. 7. (a) Axial strains during triaxial tests with various confining pressure and $\theta = 90°$. (b) Axial strains during triaxial tests with various confining pressure and $\theta = 45°$. (c) Axial strains during triaxial tests with various confining pressure and $\theta = 0°$.

axial loading. It is logical that such a closure phase is less important for higher confining pressure as most initial fractures are closed during hydrostatic loading. It is also logical to find that the closure phase in $\theta = 90°$ is more important than those in other orientations, as in this orientation, the axial stress is perpendicular to the bedding planes which are compressed. However, it is interesting to notice that even for $\theta = 0°$, such a closure phase can also be observed. This may mean that apart from the apparent bedding planes, there are also other randomly distributed fractures in the shale.

(4) All the strain curves first present hardening and then softening behaviour. The softening occurs in a very brittle manner for low confining pressures. This shows the brittle failure mode of the shale.

(5) In Fig. 8(a–c), volumetric strains vs deviatoric stress are presented. At first sight, we notice that the volumetric deformation of the shale is mainly compressive and the compressibility–dilatancy transition occurs only near peak stresses. However, a closer analysis leads us to some interesting results. The volumetric strain of the shale strongly depends on the loading orientation. Considering the tests in $\theta = 90°$, the volumetric compressibility decreases when confining pressure increases. This is explained by the fact that in this orientation, the volumetric strain is mainly due to the closure of the bedding planes and thus the extensive lateral strain is much smaller than the compressive axial strain. This phenomenon disappears in $\theta = 0°$ as in this orientation the bedding planes are parallel to the axial stress and are not therefore compressed. Thus, large and brittle dilatancy is obtained when the deviatoric stress reaches its peak value, in tests with an orientation near to $\theta = 0°$. This is due to the bursting of the bedding planes.

5. ANALYSIS OF THE ELASTIC BEHAVIOUR

The analysis of the elastic behaviour is fundamental in constitutive modelling of material. In fact, the good knowledge of the elastic behaviour allows an accurate estimation of the plastic deformation and damage in material. In general, elastic constants are determined from material responses during unloading paths. For this purpose, unloading–reloading cycles were included in triaxial tests as shown in Fig. 9(a) and (b). However, it was seen that if complete unloading was performed immediately after the axial loading phase [Fig. 9(a)], important hysteresis buckles were obtained, making it very difficult to determine the slope of the unloading or reloading curve. This hysteresis phenomenon may be the result of various factors, such as the viscous properties of the shale and different friction effects. Detailed analyses of these factors are not covered in this paper. We tried to avoid hysteresis buckles as much as possible in order to determine elastic constants easily. Therefore, a short relaxation phase was included before each unloading cycle and only a partial removal of axial stress was performed [Fig. 9(b)]. In this way, unloading and reloading curves were nearly the same and almost like a straight line. This procedure may be justified by the fact that the elastic behaviour of the shale is assumed to be instantaneous and time independent [10]. However, it is useful to notice that in order to avoid very long tests, relaxation phases were short (from 30 min to 1 hr) and thus the stabilization state of creep deformation was not fully reached.

The instantaneous elastic response of a transversely isotropic material is described by the generalized Hooke's law [3]. In the coordinate system (S_1, S_2, S_3)

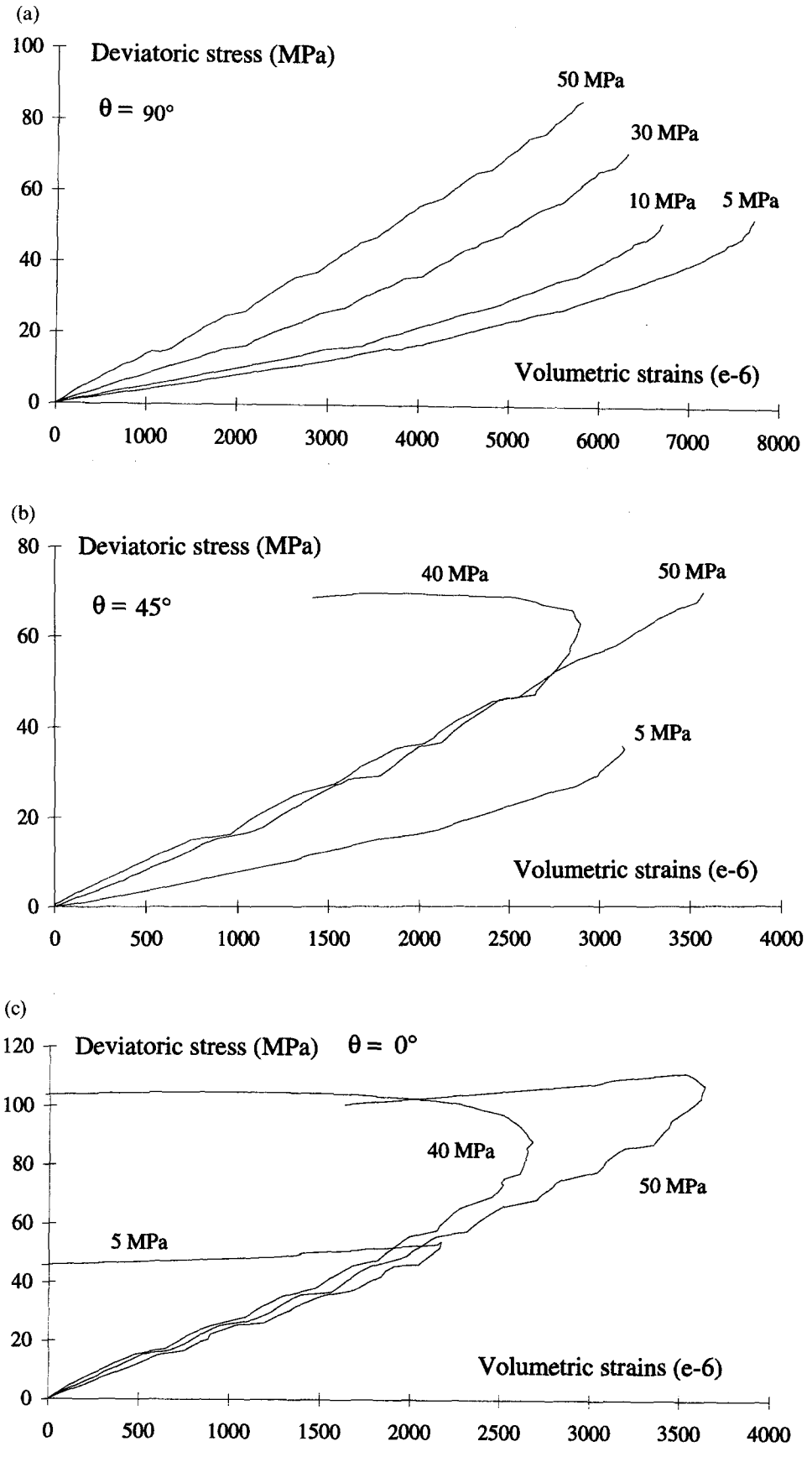

Fig. 8. (a) Volumetric strains during triaxial tests with various confining pressure and $\theta = 90°$. (b) Volumetric strains during triaxial tests with various confining pressure and $\theta = 45°$. (c) Volumetric strains during triaxial tests with various confining pressure and $\theta = 0°$.

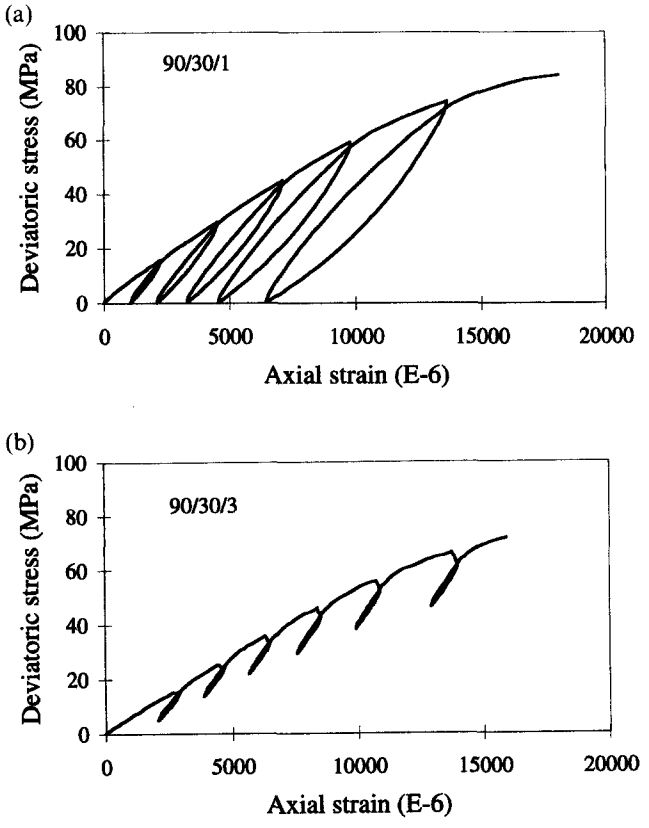

Fig. 9. (a) Stress–strain curves including unloading cycles during triaxial test without relaxation phase. (b) Stress–strain curves including unloading cycles during triaxial test with relaxation phase.

defined in Fig. 1, the stress–strain relation is given in the Voigt notation as follows:

$$\begin{bmatrix} \varepsilon_1 \\ \varepsilon_2 \\ \varepsilon_3 \\ \gamma_{23} \\ \gamma_{31} \\ \gamma_{12} \end{bmatrix} = \begin{bmatrix} \frac{1}{E_1} & -\frac{\nu_{21}}{E_2} & -\frac{\nu_{21}}{E_2} & 0 & 0 & 0 \\ -\frac{\nu_{12}}{E_1} & \frac{1}{E_2} & -\frac{\nu_{23}}{E_2} & 0 & 0 & 0 \\ -\frac{\nu_{12}}{E_1} & -\frac{\nu_{23}}{E_2} & \frac{1}{E_2} & 0 & 0 & 0 \\ 0 & 0 & 0 & \frac{1}{G_{23}} & 0 & 0 \\ 0 & 0 & 0 & 0 & \frac{1}{G_{31}} & 0 \\ 0 & 0 & 0 & 0 & 0 & \frac{1}{G_{12}} \end{bmatrix} \times \begin{bmatrix} \sigma_1 \\ \sigma_2 \\ \sigma_3 \\ \tau_{23} \\ \tau_{31} \\ \tau_{12} \end{bmatrix} . \quad (1)$$

In this equation, σ_i and ε_i ($i = 1$–3) are, respectively, the normal stress and strain in the S_i direction. τ_{ij} and γ_{ij} (i, $j = 1$–3 and $i \neq j$) denote the shear stress and strain in the plane (S_i, S_j). The elastic compliance matrix depends on five independent parameters. E_1 is the Young modulus in the S_1 direction normal to the bedding planes. E_2 is the corresponding modulus in any direction in the bedding planes which represent the isotropic plane of the shale. ν_{ij} (ν_{23}, ν_{12} or ν_{21}) is the Poisson's ratio defining the lengthening deformation in the S_j direction due to the normal stress in the S_i direction. G_{12} is the shear modulus in the (S_1, S_2) plane (Fig. 1), an independent material parameter characterizing the angular deformation between S_1 and S_2 due to the shear stress τ_{12} in the plane (S_1, S_2). G_{23} denotes the shear modulus in the (S_2, S_3) plane. As this plane is the isotropic plane of the shale, G_{23} is not an independent parameter and related to the Young modulus and Poisson's ratio (E_2, ν_{23}) by the equation $G_{23} = E_2/2(1 + \nu_{23})$. Moreover, the conservation law of energy for a hyperelastic material requires the symmetric condition $\nu_{12}/E_1 = \nu_{21}/E_2$.

The two Young's moduli E_1 and E_2 corresponding to two structural directions S_1 and S_2 (or S_3) are obtained, respectively, from tests performed in $\theta = 90°$ and $\theta = 0°$ by measuring axial strain during the unloading path. Similarly, Poisson's ratio ν_{12} is determined from tests in $\theta = 90°$ ($\nu_{12} = -\Delta\varepsilon_3/\Delta\varepsilon_1$) while ν_{21} and ν_{23} from tests in $\theta = 0°$ ($\nu_{21} = -\Delta\varepsilon_{3p}/\Delta\varepsilon_1$ and $\nu_{23} = -\Delta\varepsilon_{3//}/\Delta\varepsilon_1$). Finally, the shear modulus G_{12} can be obtained from any tests performed in an out-of-axis orientation. Indeed, by making a transformation of the coordinate system, the following equation is obtained:

$$\frac{1}{E_\theta} = \frac{\sin^4\theta}{E_1} + \left[\frac{1}{G_{12}} - 2\frac{\nu_{12}}{E_1}\right]\sin^2\theta\cos^2\theta + \frac{\cos^4\theta}{E_2} \quad (2)$$

where E_θ is the axial Young modulus which is determined from a test performed in the θ orientation. Thus, G_{12} is easily deduced from this equation.

For most rock materials, elastic parameters are generally stress dependent. In order to study the variation of the elastic parameters of the shale, an original experimental program was defined. Indeed, the unloading cycles were performed at the same fixed values of deviatoric stress for all confining pressures (Fig. 10). In this way, it was possible to evaluate the variation of the elastic parameters with the two most used invariants of the stress tensor: the mean stress $p = I_1/3$ and the

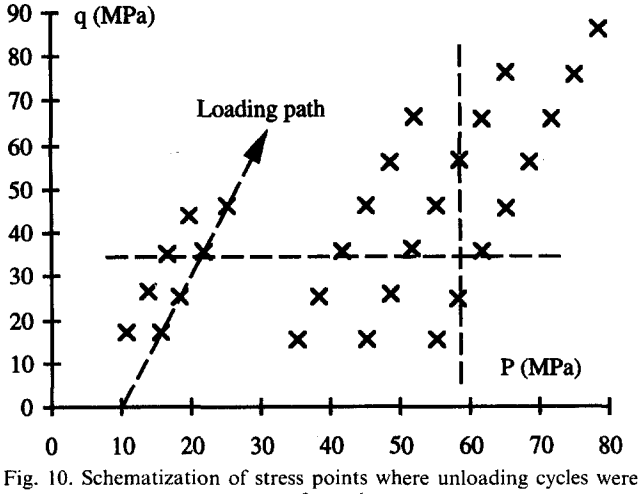

Fig. 10. Schematization of stress points where unloading cycles were performed.

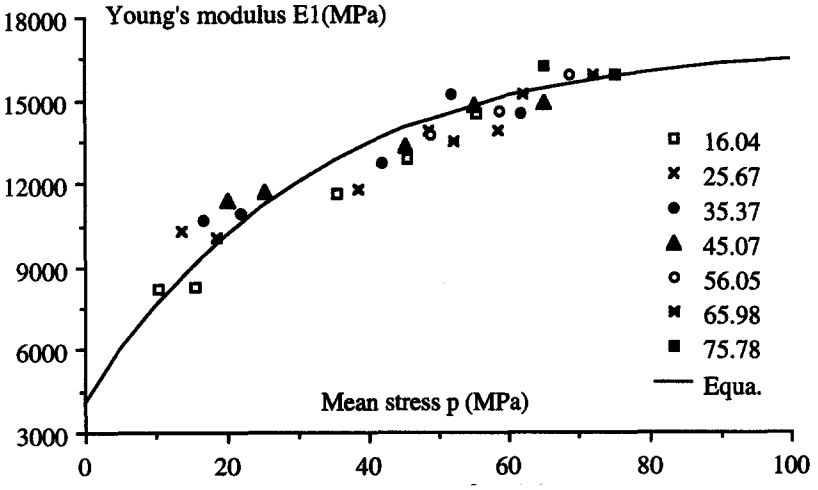

Fig. 11. Variation of Young's modulus E_1 vs the mean stress for different values of the equivalent shear stress, the continuous line is the empirical correlation.

equivalent shear stress $q = \sqrt{3J_2}$, where I_1 is the first invariant of the stress tensor and J_2 the second invariant of the deviatoric stress tensor. From a theoretical point of view, it is interesting to express the variation of elastic constants as a function of stress (or strain) invariants in order to develop non-linear hyperelastic laws.

In Figs 11–15, we present the variations of elastic parameters of the shale vs the mean stress for different levels of the deviatoric stress. All the parameters generally increase with the mean stress. This is quite common for rock materials. However, some interesting distinctions should be noticed.

First, Young's modulus E_1 increases not only with the mean stress, but also with the shear stress, and it has the largest variation among all the constants. This is obviously related to progressive closure of the bedding planes. Furthermore, even if E_2 and ν_{21} mainly depend on the mean stress, there is a slight decrease of E_2 and an increase of ν_{21} with the shear stress. As these two parameters are related to the shale behaviour in the direction parallel to the bedding planes, we can deduce that these variations may be due to induced damage in the shale matrix. Finally, it is useful to notice that all the parameters tend to lean towards a constant value (a linear elastic law) when stress levels become very high.

Let us now consider the shear modulus G_{12} (or G_{13}), which should be determined from out-of-axis tests. Experimental results obtained from these tests with different orientations showed a large scattering [9]. An average value of G_{12} was calculated for each test. Some representative values obtained from three tests in $\theta = 45°$ are presented in Table 2.

To avoid a lack of accuracy related to experimental determination of G_{12}, the well known Saint-Venant's formula is used [3, 5]:

$$\frac{1}{G_{12}} = \frac{1}{E_1} + \frac{1}{E_2} + 2\frac{\nu_{12}}{E_1}. \tag{3}$$

This equation allows us to reduce the number of elastic constants from five to four. The validity of this equation was tested for the studied shale. In Table 2, numerical average values obtained with Saint Venant's equation are compared with experimental ones. A good agreement is obtained.

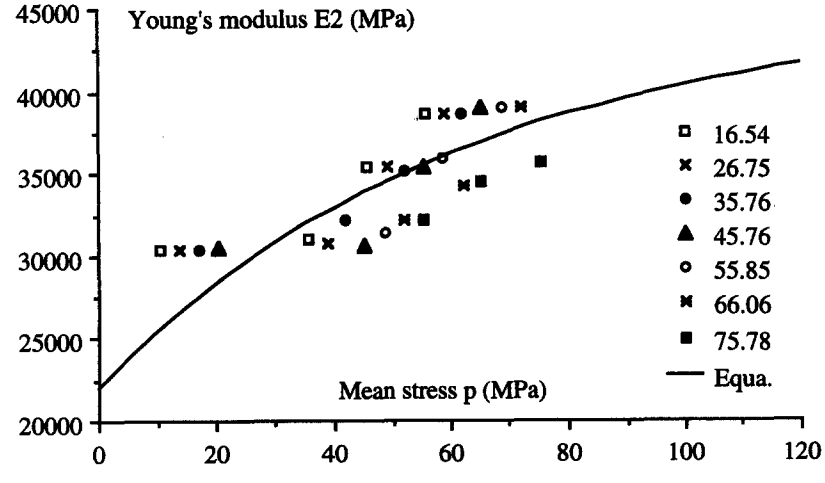

Fig. 12. Variation of Young's modulus E_2 vs the mean stress for different values of the equivalent shear stress, the continuous line is the empirical correlation.

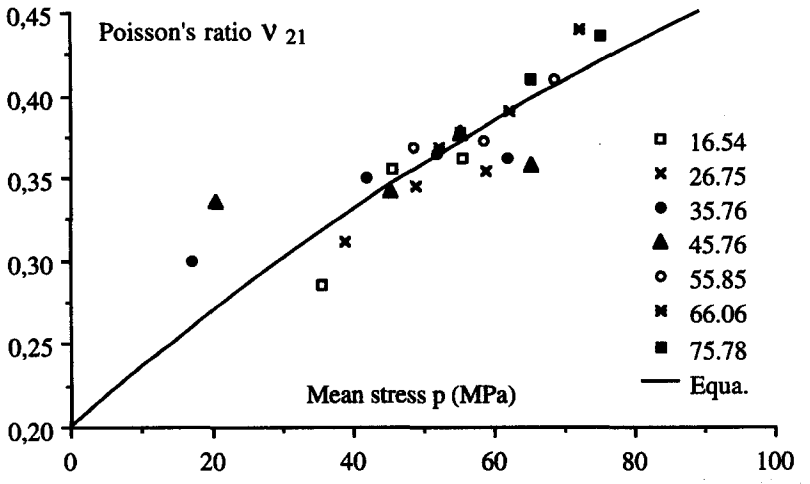

Fig. 13. Variation of Poisson's ratio v_{21} vs the mean stress for different values of the equivalent shear stress, the continuous line is the empirical correlation.

Moreover, applying Saint-Venant's formula in equation (2) and making the first derivative of E_θ with regard to θ, leads to the following equation:

$$\frac{dE_\theta}{d\theta} = \frac{-2\cos 2\theta}{(V_1 + V_2 \sin 2\theta)^2} V_2 \qquad (4)$$

with

$$V_1 = \frac{1}{2}\left(\frac{1}{E_1} + \frac{1}{E_2}\right)$$

$$V_2 = \frac{1}{2}\left(\frac{1}{E_1} - \frac{1}{E_2}\right).$$

In general, $E_2 > E_1$, we can see that if Saint-Venant's equation is applied, the axial Young's modulus E_θ should continuously decrease with the loading orientation θ. In Fig. 16, we present the average values of the axial modulus, determined at different levels of the deviatoric stress in two triaxial tests under different confining pressures. We notice that E_θ decreases actually with the loading orientation. This confirms that Saint-Venant's equation is quite well verified in the case of Tournemire shale.

Let us now discuss the last point relating to the elastic behaviour of the shale. As we mentioned above, in the framework of hyperelastic materials, the symmetry of the elastic matrix should be verified, $v_{12}/E_1 = v_{21}/E_2$. In Fig. 17, experimental values of the ratios v_{12}/E_1 and v_{21}/E_2 are given in function of the mean stress for various levels of the shear stress. It is obvious that the experimental data do not verify this symmetry and systematically we have $v_{12}/E_1 > v_{21}E_2$. However, when the mean stress becomes higher, the two ratios become closer to each other and the symmetry condition is almost verified. The dissymmetry of the experimental elastic matrix can be explained by two main factors. The first is related to initial randomly distributed faults and heterogeneities in microscopic scale and the second is due to stress induced anisotropy by damage of the shale.

As can be seen from the preceding points, the elastic deformation of the shale cannot be described by the linear elasticity theory and further information or assumptions are still necessary to establish a non-linear hyperelastic theory. However, in order to take into account the stress dependency of the elastic constants of the shale in resolution of engineering problems, here we try to give empirical equations to describe the variations

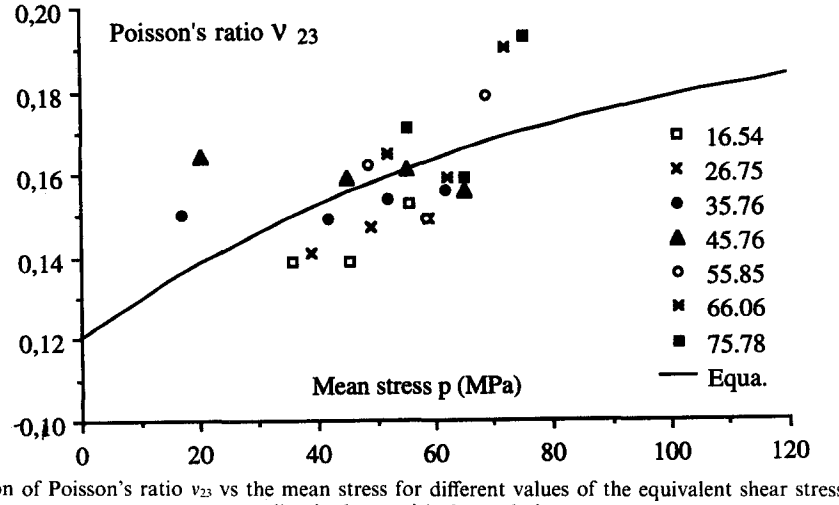

Fig. 14. Variation of Poisson's ratio v_{23} vs the mean stress for different values of the equivalent shear stress, the continuous line is the empirical correlation.

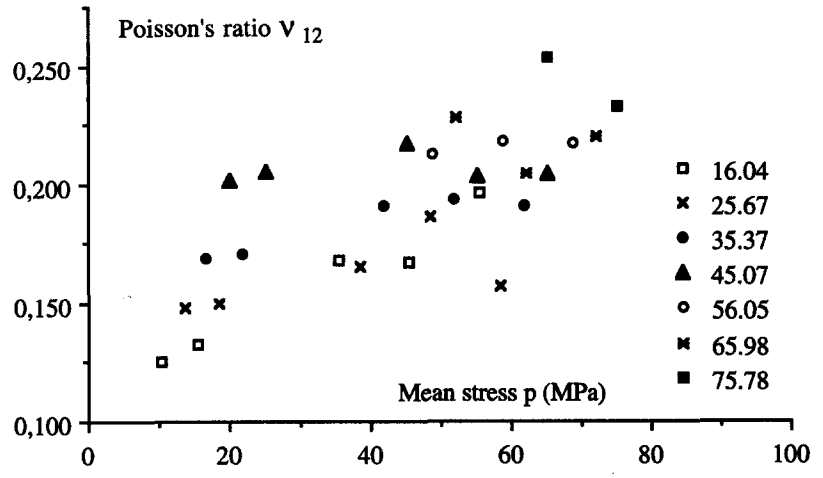

Fig. 15. Variation of Poisson's ratio v_{12} vs the mean stress for different values of the equivalent shear stress.

of the elastic parameters. For simplicity's sake and according to the experimental data obtained, it is acceptable to neglect influences of the shear stress and suggest that the elastic parameters of the shale depend on the mean stress only. Therefore, the following equations have been obtained and compared with the experimental data (Figs 11–15):

$$\begin{cases} E_1 = E_1^s(E_1^s - - E_1^0)e^{-\alpha(p/p^*)} \\ E_1^s = 17{,}000 \text{ MPa}, E_1^0 = 4000 \text{ MPa}, \alpha = 0.032 \end{cases} \quad (5a)$$

$$\begin{cases} E_2 = E_2^s - (E_2^s - E_2^0)e^{-\beta(p/p^*)} \\ E_2^s = 45{,}000 \text{ MPa}, E_2^0 = 22{,}000 \text{ MPa}, \beta = 0.016 \end{cases} \quad (5b)$$

$$\begin{cases} v_{21} = v_{21}^s - (v_{21}^s - v_{21}^0)e^{-\gamma(p/p^*)} \\ v_{21}^s = 0.75, v_{21}^0 = 0.2, \gamma = 0.0068 \end{cases} \quad (5c)$$

$$\begin{cases} v_{23} = v_{23}^s - (v_{23}^s - v_{23}^0)e^{-\lambda(p/p^*)} \\ v_{23}^s = 0.2, v_{23}^0 = 0.12, \lambda = 0.013 \end{cases} \quad (5d)$$

In these equations, the parameters with superscript "0" are the initial values of elastic parameters for $p \leq 0$ and those with superscript "s" the asymptotic values for very high stress levels ($p \to \infty$). p^* is the reference pressure to obtain dimensionless parameters. Finally, the symmetric condition of the elastic matrix and Saint-Venant's equation are applied.

6. ANISOTROPY OF STRENGTH AND FAILURE MECHANISM

A preliminary analysis of failure surface has been carried out based on the experimental data of peak stresses obtained in triaxial tests. The anisotropy of shale strength and the general form of failure surface in the stress space have been emphasized.

Table 2. Average values of the shear modulus

Confining pressure σ_3 (MPa)	G_{12} (MPa) from Saint-Venant equation	G_{12} (MPa) from tests in $\theta = 45°$
5	5886	4940
40	8013	8167
50	8349	8713

Experimental values of peak stress in triaxial tests are shown in Fig. 18 as a function of the loading orientation and for various confining pressures. One can notice that the failure stress of the shale depends on the loading orientation θ and there are two maximum values at $\theta = 0°$ and $\theta = 90°$. The minimum strength is found between $\theta = 30°$ and $\theta = 60°$. Similar results have been obtained by several authors for other kinds of rocks [11, 12].

For transversely isotropic materials, the anisotropy degree of strength is generally defined by the following two parameters:

$$k_1 = \frac{(\sigma_1 - \sigma_3)_{//}}{(\sigma_1 - \sigma_3)_{\perp}} \quad (6a)$$

$$k_2 = \frac{(\sigma_1 - \sigma_3)_{\max}}{(\sigma_1 - \sigma_3)_{\min}} \quad (6b)$$

where k_1 defines the ratio between the failure stresses in two principal directions, respectively, parallel and perpendicular to the bedding planes, and k_2 the ratio between the maximum and minimum strength. Experimental values of these two ratios for Tournemire shale

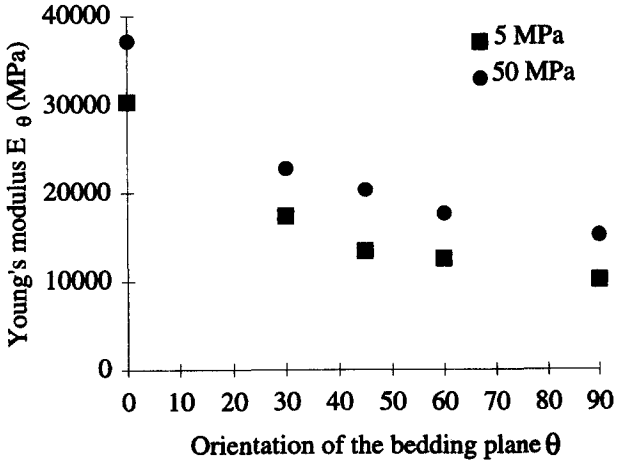

Fig. 16. Variation of axial Young modulus E_θ vs loading orientation during triaxial test with different confining pressures.

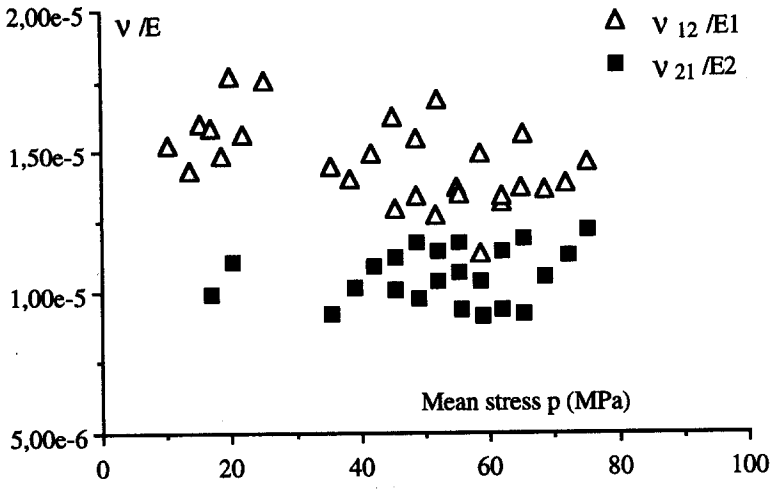

Fig. 17. Experimental verification of the symmetry of the elastic matrix.

are shown in Fig. 19. One can note that k_1 is nearly equal to 1 except for very low confining pressure, thus the strength anisotropy between the two principal structural axes is very small. The value of k_2 is about 1.5 and decreases little when confining pressure increases. This implies that the strength anisotropy becomes smaller for high confining pressure. These results are similar to those obtained for other shales, for instance, the Green River shale ($k_2 = 1.37$ [13]), the Green River shale I ($k_2 = 1.62$ [12]) and the Green River shale II ($k_2 = 1.41$ [12]).

The anisotropy of strength is related to the failure mechanism in shale. A direct analysis of fractures observed on failed samples has been carried out. A schematization of the main failure modes in function of loading orientation and confining pressure is given in Fig. 20. Generally, the fracture angle strongly depends on the loading orientation as well as confining pressure. The failure occurs in two principal modes, extension and shearing. However, fractures can develop both in shale matrix and in bedding planes. For loading orientations $15° \leq \theta \leq 60°$, the failure generally takes place because of the sliding of bedding planes and thus the fracture orientation is nearly equal to θ. However, when confining pressure is high, shear band by strain localization in shale matrix can occur and the fracture may cross bedding planes. For loading orientations near the principal structural direction S_2, $\theta \in (0°, 15°)$, the failure takes place by extension of the bedding plane for low confining pressures and by shear band in shale matrix for high confining pressures. Finally, for loading orientations near principal structural direction S_1, $\theta \in (60°, 90°)$, the failure is mainly due to shear bands in shale matrix and the fracture angle (with regard to axial stress) increases with confining pressure.

In order to complete experimental values of failure stress in triaxial tests, several proportional loading and lateral extension tests have also been carried out. Detailed data of these tests are given in ref. [9] and not presented here. In proportional tests, axial and lateral stresses are increased simultaneously with a constant ratio. In lateral extension tests, samples are first submitted to a hydrostatic stress state and then the confining pressure is decreased by keeping a constant axial stress. The whole data of failure stress from various tests are presented in the classical p–q plane, shown in Fig. 21 for two principal loading orientations. It is clear that the experimental failure surfaces are of a non-linear

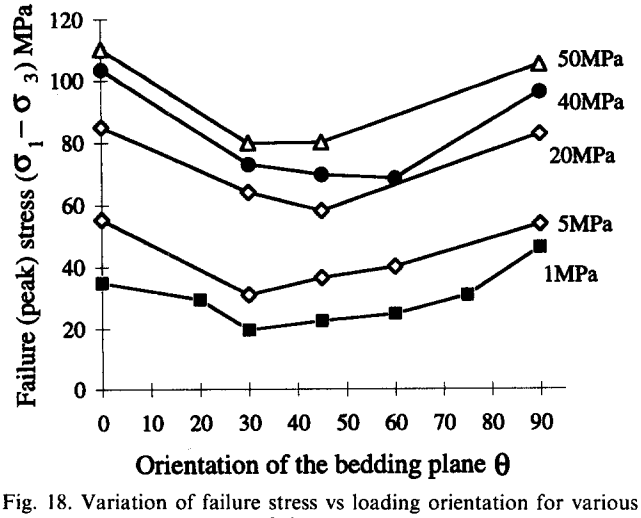

Fig. 18. Variation of failure stress vs loading orientation for various confining pressure.

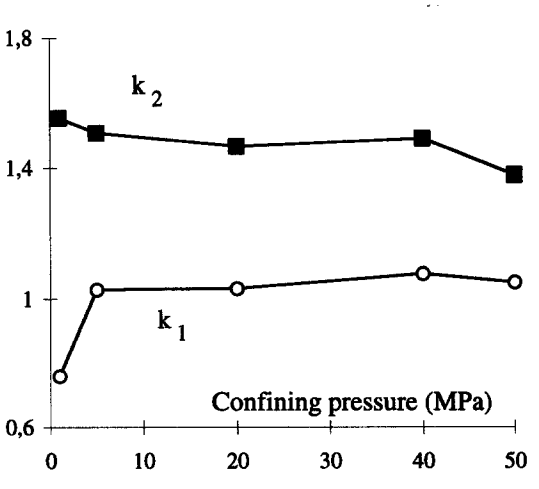

Fig. 19. Variation of anisotropy degree parameters of failure stress vs confining pressure.

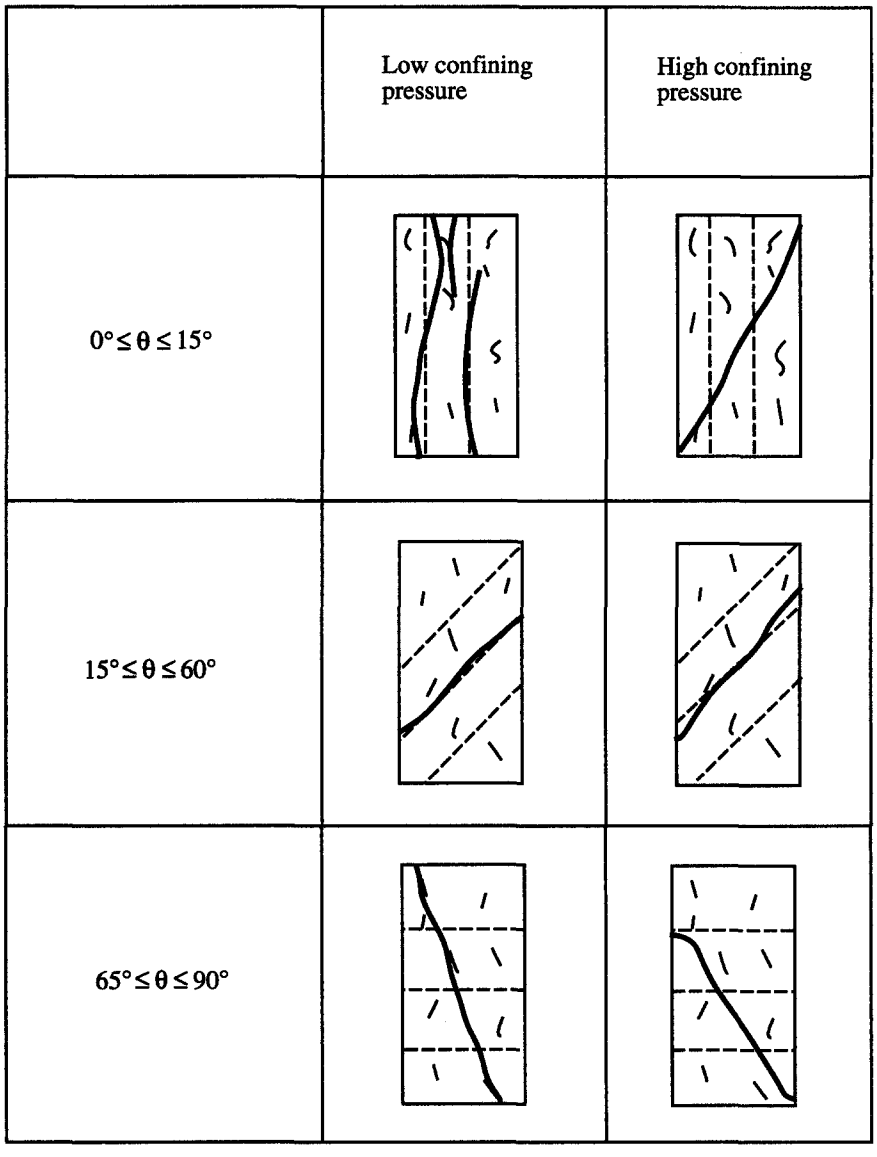

Fig. 20. Schematization of main failure modes.

form and thus a linear Mohr–Coulomb type criterion cannot be used for the shale.

7. CONCLUSIONS

The extensive experimental results of Tournemire shale during compressibility and triaxial compression tests under different confining pressure and loading orientation have been presented. These offer an original data base, necessary to establish and validate constitutive models for anisotropic rocks.

The mechanical behaviour of Tournemire shale is mainly characterized by the strong anisotropic plastic deformation. However, the anisotropy of failure strength is not very important. Influences of secondary initial faults can be neglected with regard to the bedding planes. Non-associated plastic models should be developed to describe the inelastic response of the shale. Moreover, there is initiation and growth of microcracks, yielding the degradation of the elastic properties. But in a first approach of numerical modelling, it seems acceptable to neglect the effect of the induced damage. The original experimental program allowed us to determine the variation of the elastic parameters of the shale with the two first stress invariants. The results have shown that the elastic behaviour of the shale is clearly non-linear. The symmetric condition deduced from the energy conservation law for a hyperelastic material was not verified. The development of the non-linear elastic model should be coupled with the description of induced damage. The failure mechanisms of the samples have been analyzed. The failure surfaces in the p–q plane are obviously of a non-linear form. The failure mode depends on confining pressure and loading orientation. The main mechanisms of failure are the extension and sliding of the bedding planes, the splitting and the shear bands in shale matrix. Mixed modes were often observed. The failure occurs in a brittle way, yielding a sudden collapse of shale strength. The volumetric strain is mainly compressive and the transition to dilatancy occurs only in the zone near peak stress.

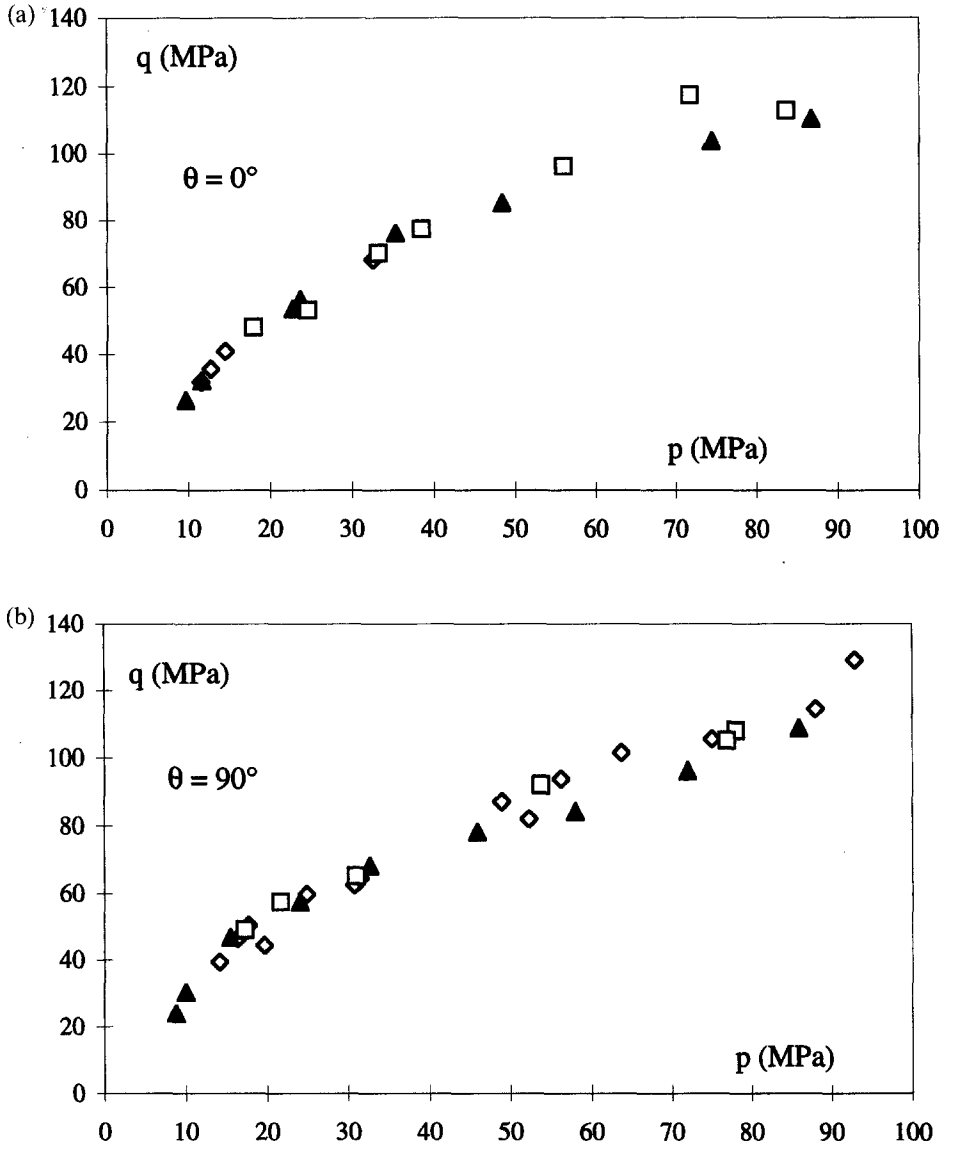

Fig. 21. (a) Experimental failure surface in p–q plane for the principal direction $\theta = 0°$. (b) Experimental failure surface in p–q plane for the principal direction $\theta = 90°$.

Finally, it is usful to notice that the time dependency of the mechanical behaviour of the shale is quite important according to relation phases included in the triaxial tests. Therefore, for long term stability study of structures, it will be necessary to develop time dependent constitutive models. Numerical modelling of the mechanical behaviour of Tournemire shale is being conducted in our on going works [14].

Acknowledgements—The authors would like to thank ELF-Aquitaine for financial support to carry out this work and permission to publish this paper. They would also like to thank Professor N. D. Cristescu for his various suggestions and Dr O. Cazacu for her precious help.

Accepted for publication 7 August 1996.

REFERENCES

1. Kwasniewski M. A. Mechanical behavior of anisotropic rocks. In *Comprehensive Rock Engineering, Vol. 1: Fundamentals*, pp. 285–312. Pergamon Press, Oxford (1993).
2. Ramamurthy T. Strength and modulus responses of anisotropic rocks. In *Comprehensive Rock Engineering, Vol. I: Fundamentals* (Edited by Hudson J. A.), pp. 313–329. Pergamon Press, Oxford (1993).
3. Lekhnitskii S. G. *Theory of Elasticity of an Anisotropic Elastic Body*. Holden Day, San Francisco (1963).
4. Boehler J. P. Lois de comportement anisotrope des milieux continus. *J. de Mécanique* **17**, 153–190 (1978).
5. Boehler J. P. Yielding and failure of transversely isotropic solids. In *Applications of Tensor Functions in Solids Mechanics: Courses and Lectures N° 292* (Edited by Boehler), pp. 67–96. CISM Udine (1987).
6. Amadei B. *Rock Anisotropy and the Theory of Stress Measurements*. Springer, Heidelberg (1983).
7. Schmitt L., Forsans T. and Santarelli F. J. Shale testing and capillary phenomena. *Int. J. Rock Mech. Min. Sci. & Geomech. Abstr.* **31**, 411–427 (1994).
8. Schmitt L. Etude du soutènement hydraulique des puits pétroliers dans les argilites par l'essai triaxial à confinement fluide direct. Doctoral thesis (in French), INPL, ENSG de Nancy (1994).
9. Niandou H. Etude du comportement rhéologique et modélisation de l'argilite de Tournemire: Applications à la stabilité d'ouvrages souterrains. Doctoral thesis (in French), Université de Lille I (1994).
10. Cristescu N. D. *Rock Rheology, Mechanics of Elastic and Inelastic Solids*. Kluwer Academic (1989).
11. Donath F. A. Effects of cohesion and granularity on deformational behavior of anisotropic rock. In *Studies in*

Mineralogy and Precambrian Geology (Edited by Doc B. R. and Smith D. K.), Vol. 135, pp. 95–128. Geological Society of America, Boulder (1972).
12. McLamore R. and Gray K. E. The mechanical behavior of anisotropic sedimentory rocks. *J. Engng Ind., Trans. ASME* **89**, 62–73 (1967).
13. Chenevert M. E. and Gatlin C. Mechanical anisotropies of laminated sedimentory rocks. *Soc. Petrol. Eng. J.* **5**, 67–77 (1965).
14. Cazacu O., Cristescu N. D., Shao J. F. and Henry J. P. Elastic/viscoplastic constitutive equation for anisotropic shale. In *Rock Mechanics: Tools and Techniques* (Edited by Aubertin *et al.*), pp. 1683–1690 (1996).